Localizing the Error Covariance by Physical Distances within a Local Ensemble Transform Kalman Filter (LETKF)

Takemasa Miyoshi[1], Shozo Yamane[2, 3], and Takeshi Enomoto[4]
[1]*Numerical Prediction Division, Japan Meteorological Agency, Tokyo, Japan*
[2]*Faculty of Risk and Crisis Management, Chiba Institute of Science, Choshi, Japan*
[3]*Frontier Research Center for Global Change, JAMSTEC, Yokohama, Japan*
[4]*Earth Simulator Center, JAMSTEC, Yokohama, Japan*

Abstract

An efficient implementation of the local ensemble transform Kalman filter (LETKF) with the error covariance localization by physical distances is introduced and assessed in this study. Instead of using local patches uniform in the model grid space to localize the error covariance, accurate physical distances are computed and used for the localization, so that the problem of analysis discontinuities in the Polar Regions is solved. Data assimilation cycle experiments with real observations are performed, which indicate less discontinuity in the Polar Regions. Moreover, the computational time is shorter and more robust for various localization scales. Thus, the implementation introduced in this study is a promising choice of future LETKF systems.

1. Introduction

The local ensemble Kalman filter (LEKF) was first proposed by Ott et al. (2002; 2004). A main advantage of LEKF is its efficiency in the parallel architecture. Moreover, LEKF computational time is robust with increasing observations (e.g., Szunyogh et al. 2005), while that of most other ensemble Kalman filter (EnKF) implementations is essentially proportional to the number of observations. Hunt et al. (2007) applied the ensemble transform Kalman filter (ETKF, Bishop et al. 2001) approach to LEKF to propose the local ensemble transform Kalman filter (LETKF), an efficient upgrade of LEKF. It is known that LETKF is several times faster than LEKF while keeping identical analysis accuracy (e.g., Harlim 2006).

A major difference between LETKF and LEKF is that LETKF does not require "local patches" (Hunt et al. 2007), thus it allows a flexible choice of observations to be assimilated at each grid point. There has been a problem of analysis discontinuity in the Polar Regions when we choose observations by the "local patches", as shown by Miyoshi and Yamane (2007, "MY07" hereafter). The original implementation of LEKF, as well as the LETKF by MY07, separates the global model grid into local patches uniformly in the model grid space. The physical length between two successive grid points in the longitudinal direction is proportional to cosine of latitude. Therefore, the physical size of the local patch in the Polar Regions is much smaller than that in lower latitudes. This causes discontinuity in the analysis, which is not preferable. To avoid this, we could increase the zonal grid points of local patches according to latitudes, which would not be efficient.

Alternatively, LETKF does not require local patches as mentioned by Hunt et al. (2007) although they did not provide a precise description of the implementation without local patches. Removing local patches from LETKF, we could apply natural localization weighting determined only by the physical distance.

Moreover, without local patches, the computation is accelerated and more robust with choices of localization scales. MY07 indicated that computational time is increased quadratic with the local patch size, which is not preferable with higher resolution models. This disadvantage is overcome by removing the local patches.

In this study, accurate physical distances between the analyzed grid point and observations are computed and used for the error covariance localization within LETKF. Details of the LETKF implementation without local patches are described for the first time. Data assimilation cycle experiments with an AGCM assimilating real observations are performed to find the effects of the natural localization. The implementation of LETKF with accurate physical distances is described in section 2. Following the description of the experimental settings in section 3, results are presented in section 4. Finally, summary and discussion are provided in section 5.

2. LETKF implementation with accurate physical distances

In the original algorithm of the LEKF by Ott et al. (2002; 2004), we define a local patch around every grid point and analyze all variables inside the local patch. However, as Hunt et al. (2007) mentioned, we no longer need local patches in the LETKF algorithm. We constitute the global analysis using analysis values at the local patch center; that is, we do not use all analysis values but those at the center point. Therefore, we need to analyze only the variables at the local patch center.

The LETKF analysis equation is given by

$$\begin{aligned}\mathbf{X}^a &= \overline{\mathbf{X}^f} + \mathbf{K}(\mathbf{y}^o - \overline{H(\mathbf{X}^f)}) + \delta\mathbf{X}^a \\ &= \overline{\mathbf{X}^f} + \delta\mathbf{X}^f[\mathbf{U}\mathbf{D}^{-1}\mathbf{U}^T(\delta\mathbf{Y}^f)^T\mathbf{R}^{-1}(\mathbf{y}^o - \overline{H(\mathbf{X}^f)}) \\ &\qquad + \sqrt{m-1}\,\mathbf{U}\mathbf{D}^{-1/2}\mathbf{U}^T], \end{aligned} \tag{1}$$

where we define the eigenvalue decomposition:

$$(m-1)\mathbf{I} + (\delta\mathbf{Y}^f)^T\mathbf{R}^{-1}\delta\mathbf{Y}^f = \mathbf{U}\mathbf{D}\mathbf{U}^T, \tag{2}$$

(cf., Hunt et al. 2007). Here, $\mathbf{X}$ and $\delta\mathbf{X}$ denote $N \times m$ matrices whose columns are composed of ensemble members and perturbations, respectively, where N and m indicate the system dimension and ensemble size. Superscripts indicate analysis (a) and forecast (f). H denotes a generally nonlinear observational operator which operates an N-dimensional state vector to return a p-dimensional observational vector, where p denotes the number of observations (the dimension of the observational space). When H is applied to an $N \times m$ matrix $\mathbf{X}$, each column of $\mathbf{X}$ is transferred by H to return a $p \times m$ matrix. Overbar returns a vector composed of the ensemble mean for each row. $\delta\mathbf{Y} = H(\mathbf{X}) - \overline{H(\mathbf{X})}$ indicates ensemble perturbations in the observational space. $\mathbf{R}$ denotes a $p \times p$ matrix composed of the observational error covariance. If observations are uncorrelated, which is a common assumption, $\mathbf{R}$ is diagonal, thus the inverse is trivial. According to eqn. (1), the $m \times m$ trans-

Corresponding author: Takemasa Miyoshi, Numerical Prediction Division, Japan Meteorological Agency, 1-3-4 Otemachi, Chiyoda-ku, Tokyo 100-8122, Japan. E-mail: miyoshi@naps.kishou.go.jp.

formation matrix **T**:

$$\mathbf{T} = \mathbf{U}\mathbf{D}^{-1}\mathbf{U}^T(\delta\mathbf{Y}^f)^T\mathbf{R}^{-1}(\mathbf{y}^o - \overline{H(\mathbf{X}^f)}) + \sqrt{m-1}\,\mathbf{U}\mathbf{D}^{-1/2}\mathbf{U}^T, \quad (3)$$

is what we compute for the LETKF data assimilation. In order to obtain **T**, we do not need to store vectors or matrices with dimension N. Once we compute $\delta\mathbf{Y}^f$ and $H(\mathbf{X}^f)$, we redefine the dimension of **X** as the number of variables at a grid point (usually less than 10) to solve eqn. (1).

In summary, when we analyze variables for the grid point (i', j', k'), for example, we can choose any observation without using the local patch, which determines the observational space, i.e., $\delta\mathbf{Y}^f$ and $H(\mathbf{X}^f)$. Then, we compute the $m \times m$ transformation matrix **T** to analyze the variables for the grid point (i', j', k'). Here, eqn. (1) is solved only for the variables at the grid point (not in the local patch), namely, the dimension of each column of $\mathbf{X}^a$, $\mathbf{X}^f$, and $\delta\mathbf{X}^f$ is just the number of variables at the grid point (i', j', k').

This implementation without local patches significantly accelerates the LETKF. Furthermore, it allows a flexible choice of observations to be assimilated for a grid point. Here, observation localization (Hunt et al. 2007; MY07), multiplying the inverse of the localization function to the observational error covariance, plays an essential role. In the implementation in this study, the localization weights are given by the Gaussian function:

$$w(r) = \exp\left(-\frac{r^2}{2\sigma^2}\right), \quad (4)$$

where the localization length σ is defined in physical length (m). The distance r between the local patch center and observation whose positions are given by longitudes and latitudes is computed using Hubeny's law (Hubeny 1953):

$$r = \sqrt{(A \cdot dP)^2 + (B \cdot \cos P \cdot dR)^2}, \quad (5)$$

where P, dP, and dR denote average latitude, differences of latitude and longitude, respectively. A and B indicate curvature radii of the prime meridian and prime vertical circle, computed by

$$A = \frac{R_{po}}{(1 - e \cdot \sin^2 P)^{3/2}}, \quad (6)$$

$$B = \frac{R_{eq}}{(1 - e \cdot \sin^2 P)^{1/2}}. \quad (7)$$

Here, the short and long axes of the Earth R_{po} = 6334834.0 m and R_{eq} = 6377937.0 m are used, and e = 0.006674 is a constant. This formula gives more accurate distance with less computational cost than the commonly used spherical triangle method. One can further accelerate by assuming the sphere Earth, i.e., e = 0 and $R_{po} = R_{eq}$. Although eqn. (4) has infinitely long tails, we truncate the tails to simulate the fifth-order piecewise rational function by Gaspari and Cohn (1999) (cf., Hamill et al. 2001), which is a widely used localization weighting function in EnKF studies. The fifth-order rational function drops to zero at

$$\mathrm{r} = 2 \cdot \sqrt{\frac{10}{3}} \cdot \sigma. \quad (8)$$

We force zero covariance, i.e., do not assimilate observations, beyond the distance. This is equivalent to choosing observations by a circular local patch with a constant radius in the physical space. This may introduce slight discontinuity, which can be ignored considering that choosing observations with the original local patches (uniform squares in the model grid space) would cause more evident discontinuity at the edges of the local patches.

A technical problem is the computational cost in searching observations to be assimilated at each grid point and computing accurate distances. Due to the large number of grid points, the search efficiency is essential in the algorithm. In this study, we make two-dimensional sorting of the observational data and store the address (array index) of the observational data arrays at each grid point. The original idea is coming from the JMA operational optimal interpolation (OI) system (JMA 2002). Figure 1 shows a schematic of the array indices at each grid point. Observational data arrays are sorted horizontally with the sort sequence starting at the lower left corner of the model grid and going to right. If the sequence reaches the right end, it continues to one grid up at the left end. The sequence finishes at the upper right corner. The index array with the size of the model grid stores the accumulated number of observations as shown in Fig. 1. In this way, if we search observations at a specific grid point, we just see the index numbers of the grid point and the previous grid point, say i and j, respectively. The difference of the index numbers, i.e., $i - j$, indicates the number of observations in the grid point. If $i - j$ is not zero, we refer the array indices from $j + 1$ to i. A similar approach is applied in searching observations in a specific range of grid points in the x direction, where we take the starting index j from the previous grid point of the first one and take the final index i from the final grid point. Thus, the search time is not dependent on the number of observations, although the required one-time sorting time depends on the number of observations. We can take advantages of parallel processing to accelerate the one-time sorting, which is efficient with a large number of computational nodes. In this study, MY07's parallel implementation is applied, where the global grid is separated horizontally into the number of nodes for parallel processing. Observations only necessary in each computational node are read in. Thus, the number of observations sorted in each node becomes smaller, so that sorting time is reduced.

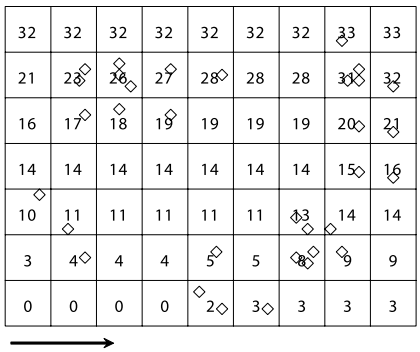

Fig. 1. A schematic showing indices of observational data array at each grid point for efficient search process. The grid corresponds to the model grid and the rhombus shows observations.

In summary, first we make a rough selection of observations by choosing nearby grid points around a grid point to be analyzed, say (i', j', k'), for example. The "nearby" grid points are determined by the physical distance by which the localization weight drops to zero (cf., eqn. (8)). The rough selection procedure is optimized by the two-dimensional sorting and greatly reduces the number of observations. Then, accurate distances from (i', j', k') are computed for all selected observations; thus, accurate distances are computed as few as possible. Finally, we apply weighting function eqn. (4) for the error covariance localization.

3. Experimental settings

The AFES-LETKF system used by MY07 is employed in this study. The MPI/OpenMP-parallelized FORTRAN90 codes developed by MY07 are modified

for the implementation with accurate physical distances described in the previous section. The model used in this study is the AFES (AGCM for the Earth Simulator, Ohfuchi et al. 2004) version 2.2 with a T159/L48 resolution, corresponding to a grid of $480 \times 240 \times 48$, which is the same as what MY07 used with real observations.

The observational data except satellite radiances in August 2004 are assimilated. The observational data including observational error settings are adapted from Japan Meteorological Agency (JMA)'s operational dataset with quality control flags. Observations only used in JMA's operational global analysis are assimilated in this study. The data includes surface pressure reports, radiosondes, wind profilers, aircraft reports, AMVs (atmospheric motion vectors), sea surface winds by QuikSCAT, dropsondes, manually derived sea-level pressure data in the SH by the Australian Bureau of Meteorology. The initial ensemble members are chosen randomly from the long-term free run of the AFES in a similar season. The observational data are assimilated every 6 hours with hourly slots. The experimental period is from 00 UTC 1 August 2004 to 18 UTC 31 August 2004. No initialization procedure is employed. These experimental conditions are the same as what MY07 did with real observations.

Two data assimilation cycle experiments are performed in this study: one with the original LETKF that MY07 developed (control experiment), and the other with the new implementation developed in this study without local patches (test experiment). The localization parameters in the control experiment are chosen to be the same as MY07, that is, $21 \times 21 \times 13$ local patch (about 800-km radius) and 6.0-grid (about 480 km) horizontal and 3.0-grid vertical Gaussian localizations. The localization scale in the test experiment is chosen to be 500 km. The vertical localization in the test experiment is chosen to be 3.0-grid, but the localization is performed in the same manner as the horizontal localization; i.e., the weighting function is smoothly damped to zero without local patches. For both experiments, 40 ensemble members are employed, and the inflation parameter is fixed to be 10% spread inflation (21% covariance inflation). The results of two experiments are compared to find relative advantages of the new implementation with accurate physical distances.

4. Results

Figure 2 shows ensemble spread fields for the control and test experiments on 00UTC 1 August 2004, after the first data assimilation step. Here, we see discontinuities of a rectangular shape in the Polar Regions in the control experiment, which is caused by the local patches. In the test experiment, there is no such discontinuity. In addition, since we extract more information from each observation, the ensemble spread is smaller in the Polar Regions. Even in the stabilized stage of the LETKF, the control experiment shows discontinuities of a rectangular shape in the Polar Regions, mostly near the North Pole. Figure 3 shows the analysis fields on 12UTC 16 August 2004 after an initial spin-up period. The differences of analysis fields against JMA operational analysis indicate smaller values near the Poles in the test experiment. Moreover, the differences from the JMA analysis indicate discontinuous edges near the Poles in the control experiment. MY07 investigated the dynamical balance of the analysis with local patches and indicated that no spurious dynamical waves were excited. Therefore, smoothing the discontinuities in the Polar Regions is not an advantage by removing the local patches in terms of the dynamical balance problem. The temporally averaged zonal mean of the root mean square differences against JMA analysis is computed and plotted in Fig. 4. Clear advantages of the test experiment are observed near the North Pole.

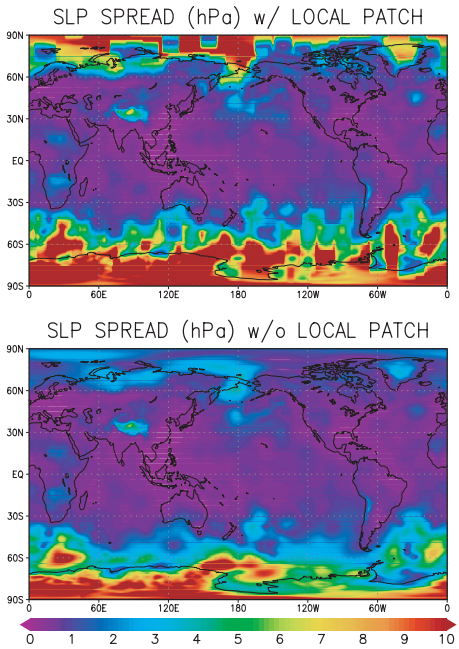

Fig. 2. Ensemble spread of sea-level pressure (hPa) on 00 UTC 1 August 2004 with the original LETKF (top, control experiment) and the modified LETKF without local patches (bottom, test experiment).

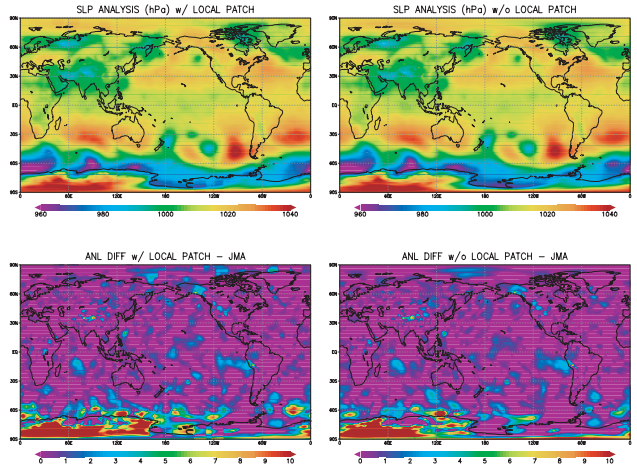

Fig. 3. Analysis fields (top) and the differences from JMA operational analysis (bottom) of sea-level pressure (hPa) on 12 UTC 16 August 2004 with the original LETKF (left, control experiment) and the modified LETKF without local patches (right, test experiment).

Advantages near the South Pole are not so large, but mid-latitudes in the Southern Hemisphere indicate clear advantages. Other areas do not show significant changes. Although Figs. 2–4 show only sea-level pressure, the results are generally true for other variables at other levels.

Timing is measured for three different localization scales for both control and test experiments. Table 1 shows the results, where the test experiment is faster than the control experiment. Moreover, timing of the test experiment is more robust with the choice of localization scales. According to MY07, the computational time of the original LETKF with local patches increases quadratic with the local patch size. Since the local patch

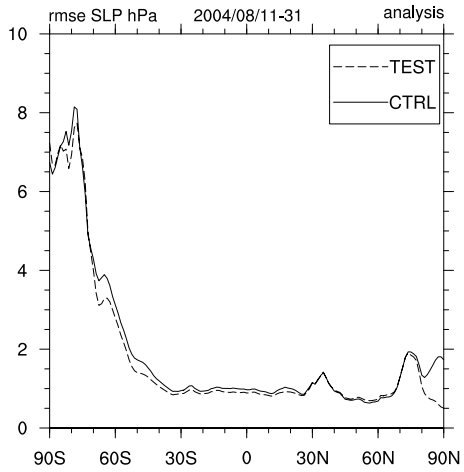

Fig. 4. Zonal mean of the root mean square differences against JMA operational analysis of sea-level pressure (hPa) for the control (solid) and test (dashed) experiments, temporally averaged for 21 days from 11 to 31 August 2004.

Table 1. Timing (sec.) of 40-member LETKF on the Earth Simulator with 40 computational nodes.

Local patch size or Localization scale	13×13×13 300 km	21×21×13 500 km	29×29×13 700 km
Original LETKF	250	425	676
LETKF without local patches	106	156	182

is not used in the new implementation, the computational time does not depend much on the choice of localization scales. This is preferable in higher resolution experiments, since the physical length between successive grid points becomes shorter, thus the local patch size tends to be larger.

5. Summary and discussion

An efficient implementation of the LETKF with accurate physical distances is proposed and assessed in this study. The data assimilation experiments with real observations indicate that the new implementation creates better analysis with less discontinuity in the Polar Regions. In addition, the computational time is faster and more robust with localization scales, which is preferable, especially for higher resolution models. Furthermore, the number of localization tuning parameters is reduced to be only the physical localization length scale. Thus, the new implementation is a promising choice of future LETKF systems.

When local patches are removed, we are flexible to choose observations. In the current implementation, the choice of observations is fixed with the physical localization length. However, in general, the flow-dependent error covariance has a skewed shape, so that the covariance spreads longer (or shorter) in some specific directions. We could consider the flow-dependence in choosing the localization weights and observations to be assimilated. There is an attempt of such flow-dependent localization, known as the hierarchical ensemble filter by Anderson (2007). The flow-dependent localization is a possible future direction to refine the algorithm.

Acknowledgments

We are grateful to members of the chaos group at the University of Maryland, especially Profs. Eugenia Kalnay, Eric Kostelich, Brian Hunt, and Dr. Istvan Szunyogh for insightful discussions. We also thank Dr. Wataru Ohfuchi of ESC, and Kohei Aranami, Yoshiaki Takeuchi, Ko Koizumi and Makoto Nishijima of NPD/JMA for kind understanding and support for this project. We used the Earth Simulator under support of JAMSTEC.

References

Anderson, J. L., 2007: Exploring the need for localization in ensemble data assimilation using a hierarchical ensemble filter. *Physica D*, **230**, 99–111.

Bishop, C. H., B. J. Etherton, and S. J. Majumdar, 2001: Adaptive sampling with the ensemble transform Kalman filter. Part I: Theoretical aspects. *Mon. Wea. Rev.*, **129**, 420–436.

Gaspari, G., and S. E. Cohn, 1999: Construction of correlation functions in two and three dimensions. *Quart. J. Roy. Meteor. Soc.*, **125**, 723–757.

Hamill, T. M., J. S. Whitaker, and C. Snyder, 2001: Distance-dependent filtering of background error covariance estimates in an ensemble Kalman filter. *Mon. Wea. Rev.*, **129**, 2776–2790.

Harlim, J., 2006: Errors in the initial conditions for numerical weather prediction: a study of error growth patterns and error reduction with ensemble filtering. Ph.D. dissertation, University of Maryland, 76 pp.

Hubeny, K., 1953: Isotheme Koordinatensysteme und konforme Abbildungen des Rotationsellipsoids. Osterr. Verein f. Vermessungswesen, Sonderheft 13, Wien, 208 S.

Hunt, B. R., E. J. Kostelich, and I. Szunyogh, 2007: Efficient data assimilation for spatiotemporal chaos: A local ensemble transform Kalman filter. *Physica D*, **230**, 112–126.

Japan Meteorological Agency, 2002: *Outline of the operational numerical weather prediction at the Japan Meteorological Agency*. available from the Japan Meteorological Agency, 158pp.

Miyoshi, T., and S. Yamane, 2007: Local ensemble transform Kalman filtering with an AGCM at a T159/L48 resolution. *Mon. Wea. Rev.*, in press.

Ohfuchi, W., H. Nakamura, M. K. Yoshioka, T. Enomoto, K. Takaya, X. Peng, S. Yamane, T. Nishimura, Y. Kurihara, and K. Ninomiya, 2004: 10-km mesh meso-scale resolving simulations of the global atmosphere on the Earth Simulator: Preliminary outcomes of AFES (AGCM for the Earth Simulator). *J. Earth Simulator*, **1**, 8–34.

Ott, E., B. R. Hunt, I. Szunyogh, M. Corazza, E. Kalnay, D. J. Patil, J. A. Yorke, A. V. Zimin, and E. J. Kostelich, 2002: Exploiting Local Low Dimensionality of the Atmospheric Dynamics for Efficient Ensemble Kalman Filtering. arXiv:physics/0203058v3.

Ott, E., B. R. Hunt, I. Szunyogh, A. V. Zimin, E. J. Kostelich, M. Corazza, E. Kalnay, D. J. Patil, and J. A. Yorke, 2004: A local ensemble Kalman filter for atmospheric data assimilation. *Tellus*, **56A**, 415–428.

Szunyogh, I., E. J. Kostelich, G. Gyarmati, D. J. Patil, B. R. Hunt, E. Kalnay, E. Ott, and J. A. Yorke, 2005: Assessing a local ensemble Kalman filter: Perfect model experiments with the NCEP global model. *Tellus*, **57A**, 528–545.

Manuscript received 21 May 2007, accepted 14 August 2007
SOLA: http://www.jstage.jst.go.jp/browse/sola/